Int. J. Electrochem. Sci., 16 **(2021)** 210240, doi: 10.20964/2021.02.31

International Journal of
ELECTROCHEMICAL
SCIENCE
www.electrochemsci.org

In-Situ and Real-Time Monitoring of Oxygen Evolution during Kolbe Reaction by Scanning Electrochemical Microscopy

Zemin Yu[1], *Yuanbo Wang*[1,2], *Xingyan Cao*[2], *Yihan Li*[2], *Tianen Ma*[2], *Liqiu Zhang*[2,*], *Lichun Liu*[2], *Hongyan Yue*[1,*]

[1] School of Materials Science and Engineering, Harbin University of Science and Technology, Harbin 150040, China.
[2] Nanotechnology Research Institute & College of Biological, Chemical Science and Engineering, Jiaxing University, Jiaxing, 314000, China
[*]E-mail: liqiu0524@zjxu.edu.cn, hyyue@hrbust.edu.cn

Received: 9 November 2020 / *Accepted:* 12 December 2020 / *Published:* 31 December 2020

In this study, the oxygen evolution during the Kobe reaction was *in-situ* and real-time monitored by scanning electrochemical microscopy (SECM) in tip-generation substrate-collection (TG/SC) mode. A typical Kolbe reaction involving the acetate electro-oxidation was used as a study model. To this end, the TG/SC method of acetate electro-oxidation was performed at a 10 μm-diameter tip Pt disk microelectrode positioned ~1.2 μm away from a 50 μm-diameter substrate Pt disk microelectrode. The substrate Pt was employed as an efficient catalyst to monitor the byproduct O_2 produced at the tip by the catalytic reduction at an appropriate electrode potential. The linear scanning voltammetry (LSV) results indicated that O_2 evolution during acetate oxidation depended on both the electrode potential and acetate concentration. At low potentials (<2.4V vs. Ag/AgCl), the current of O_2 evolution dominated the acetate oxidation reaction in 0.1 M $HClO_4$ electrolyte, while O_2 evolution was inhibited at the joint condition of higher potentials (>2.4V) and elevated concentrations of acetate, resulting in better current efficiencies of acetate oxidation. The inhibition effect of O_2 evolution was also confirmed in alkaline electrolytes, consistent with the reported literature dealing with other traditional detection techniques. In sum, the proposed detection technique based on *in-situ* and real-time dynamic monitoring of oxygen evolution was accurate and sensitive, thereby promising for the study of broad range of reactions involving the generation of oxygen species.

Keyword: Microelectrodes, Kolbe reaction, oxygen evolution, SECM, TG/SC

1. INTRODUCTION

Hydrocarbon molecules can be electrochemically synthesized at the anode through the oxidization of carboxylate anions in aqueous solutions, known as the Kolbe reaction [1-7]. During this

reaction, oxygen species are unavoidably involved as a byproduct since the electrode potential is above that required for water electrolysis (1.23 V vs. SHE). However, *in-situ* and real-time monitoring of O_2 evolution are scarce and not well reported. Therefore, the development of *in-situ* and real-time methods for proper investigation of the oxygen evolution behavior is highly desirable for a better understanding of the reaction processes and optimization of the electro-oxidation conditions for achieving better reaction efficiencies. In the past, researchers have used scale experiments to investigate the kinetics of the by-product O_2 during the Kolbe reaction at various electrode potentials by additional equipment, such as gas chromatography [8]. Such strategies are rather tedious, inefficient, and less accurate since they rely on complex *ex-situ* and asynchronous operation. By contrast, *in-situ* and real-time detection of O_2 during Kolbe reaction would be more preferred due to the convenience, high efficiency, and better accuracy.

Scanning electrochemical microscopy (SECM) is a powerful technique for probing the environment around microscale spaces using tip generation and substrate collection (TG/SC) mode [9-11]. The use of microelectrodes (Φ<50 μm) would ensure closer positioning between the tip and the substrate electrode. The TG/SC technique of SECM integrates two microelectrodes closely positioned, in which one captures the products generated from the other microelectrode. In TG/SC, a tip microelectrode (tip) is used for the oxidation or reduction reactions, and a substrate microelectrode (sub) is employed for the detection of the products generated at the tip. The generation and collection of products could be monitored *in-situ* and real-time by freely controlling the electrode potential or current. This kind of detection strongly depends on how small the distance between the tip and substrate. For instance, Kai et al. used TG/SC method to detect intermediate products of $CO_2^{\cdot-}$ radicals involved during the electrochemical reduction of carbon dioxide in N,N-dimethylformamide [12]. The long lifetimes of the radicals combined with the short distance between the tip and substrate are key factors in the successful detection of radicals. On the other hand, TG/SC method is extensively used in corrosion studies [13-16].

In this work, the TG/SC method was utilized for *in-situ* and real-time monitoring of dynamically generated oxygen species during the Kolbe reaction using linear scanning voltammetry (LSV) and SECM. The O_2 molecules generated from acetate oxidation at a Pt tip were monitored by a Pt substrate. The results showed that the rate of O_2 evolution was not directly proportional to the applied electrode potential and the concentration of acetate. At the joint condition of higher oxidation potential and elevated concentration of acetate, the O_2 evolution was almost suppressed, and the efficiency of the Kolbe reaction significantly improved.

2. EXPERIMENTAL

2.1 Materials and chemicals

Sodium acetate (CH_3COONa), sodium hydroxide (NaOH), sodium perchlorate ($NaClO_4$), perchloric acid ($HClO_4$), sulfuric acid, potassium chloride (KCl), hexaamminuruthenium (III) chloride ($[Ru(NH_3)_6]Cl_3$, RuHex), and Pt wires (99.99%) were all of reagent-grade obtained from Sigma-

Aldrich and used as received without further purification. Borosilicate glass capillaries (O.D. 2 mm, I.D. 1.16 mm) were purchased from Sutter Instrument. All solutions were prepared with deionized (DI) water (18.2 MΩ·cm^{-1}) obtained from a Milli-Q water purification system. All electrochemical experiments were carried out after purging high-purity inert He gas for at least 30 min to eliminate the dissolved oxygen.

2.2 Equipment

Scanning electrochemical microscopy (SECM 920D, CH Instrument) was used for data acquisition. Pt disk microelectrodes with diameters of 10 μm and 50 μm were used as the tip and substrate, respectively. A Pt wire was employed as a counter electrode and Ag/AgCl (1 M KCl) as a reference electrode. The Pt substrate microelectrode was mounted at the bottom of a Teflon electrochemical cell. Next, two disk microelectrodes were set in close contact with each other at a distance of ~1.2 μm. The final setup is schematically displayed in Figure 1 (cell not shown).

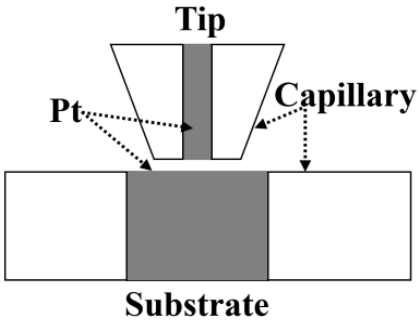

Figure 1. Structural scheme showing the tip and substrate disk microelectrodes.

2.3 Methods

2.3.1 Microelectrode fabrication

Glass capillary encapsulated Pt microelectrodes were fabricated by the methods reported in the literature [17]. Typically, one end of a 10 cm capillary was first sealed by methane-oxygen firing. A 1 cm Pt micro-wire was then carefully placed inside a capillary from the open end to the sealed end. After vacuuming the capillary, about 0.5 cm Pt wire was further sealed by electric coil heating. Next, Ag conductive glue was injected into the capillary, and a Cu wire was inserted into the conductive glue. The glue was consolidated in a 120^{o}C oven for 2 h to produce an electrical connection. The cross-section of the microelectrode was similar to that shown in Figure 1.

Sandpapers were employed for glass removal from the sealed end until exposure of the Pt wire at the flat glass surface. The whole polishing process was completed with the assistance of an optical microscope.

3. RESULTS AND DISCUSSION

3.1 Tip and substrate microelectrodes positioning and testing

In this work, a tip microelectrode was prepared by borosilicate glass capillary encapsulation followed by tip polishing to a small RG value ~3. Note that RG was defined as the ratio of the tip diameter (including the glass sheet) to the inside wire diameter. The substrate microelectrode was encapsulated using a 2 mm-diameter borosilicate glass capillary (length ~7 cm) polished to a relatively smooth surface. Under naked eyes, two microelectrodes were coarsely arranged face-to-face and an electrolyte containing 10 mM RuHex and 0.1 M KCl was injected into the cell. Negative feedback was used to move the tip to the substrate for closely approaching the two microelectrodes. The movement of the tip was stopped when the current at the constant potential of -0.3 V ($Ru^{3+}+e^{-}\rightarrow Ru^{2+}$) showed a quick decrease due to the strong limitation in ion diffusion to the tip. At such a small distance, the products produced at one microelectrode were readily captured by the other. To determine the accurate position between the two microelectrodes, positive feedback was employed. A constant potential of -0.3 V was applied to the tip and 0 V was employed to the substrate ($Ru^{2+}-e^{-}\rightarrow Ru^{3+}$). In this setup, the electric currents at both the tip and substrate underwent a dramatic increase when approached within micrometers.

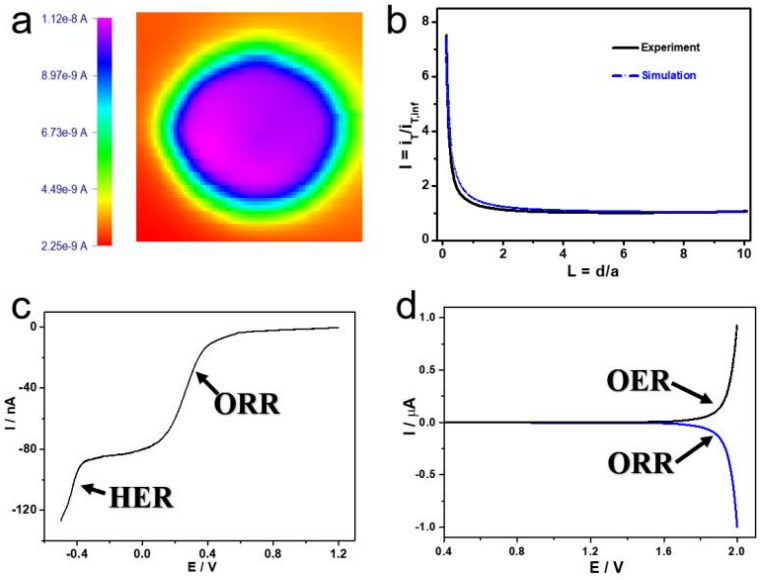

Figure 2. (a) SECM imaging of a 50 μm substrate microelectrode used for positioning of the probe and substrate microelectrodes. (b) A typical negative approach curve. (c) Linear scanning voltammogram of a 10 μm Pt microelectrode in 0.1 M $HClO_4$ electrolyte. (d) Linear scanning voltammogram obtained in generation and collection mode in 0.1 M $HClO_4$ electrolyte. Conditions: substrate potential of 0 V and scan rate of 50 mV/s.

To find the substrate, a line-by-line scanning was first conducted and then determined when an increase in current was recorded as a result of consumption of ions generated at the tip by the substrate.

This type of measurement was denoted as positive feedback. Upon establishment of the feedback between the tip and substrate, SECM imaging of the substrate was performed to precisely locate the tip at the concentric position above the substrate (Figure 2a). The precise positioning between the tip and substrate allowed the determination of the relative distance (d~1.2 μm) by fitting the positive feedback equation to an approaching curve (Figure 2b).

To acquire a proper potential of O_2 reduction, LSV was used, and the cathodic scanning from 1.2 V to -0.5 V in 0.1 M $HClO_4$ electrolyte is shown in Figure 2c. Clear current steps induced by the oxygen reduction reaction (ORR) and hydrogen evolution reaction (HER) were noticed, suggesting the effective reduction of O_2 at potentials between -0.37 V and 0.08 V in 0.1 M $HClO_4$ electrolyte.

TG/SC is a powerful technique in SECM [10, 18], which strongly depends on how close the tip and substrate were so that the products produced at the tip microelectrode can effectively be probed by the substrate microelectrode. To sensitively probe the generated products at the tip, the size of the substrate microelectrode was set to slightly larger than that of the tip. The feasibility of using the substrate to probe O_2 generated at the tip was next investigated, and the results are provided in Figure 2d. Symmetrical LSV curves corresponding to OER and ORR were obtained. The close proximity between the two microelectrodes combined with the fast diffusion of gas molecules and good catalytic activity of Pt [19] led to immediate reduction of tip generated O_2 molecules at the substrate at the potential of 0 V. Hence, TG/SC experimental results suggested that the proposed method was useful for *in-situ* and real-time monitoring of changes in O_2 concentration near the substrate.

3.2 Acetate electro-oxidation

Acetate electro-oxidation is a typical Kolbe reaction [20]. During acetate electro-oxidation, large numbers of radicals would be generated and could combine to yield symmetrical dimers and/or unsymmetrical coupling alkanes. The mechanism of acetate electro-oxidation can be summarized by the reactions below [8, 21-23]:

$CH_3COO^- \rightarrow CH_3COO\cdot + e^-$

$CH_3COO\cdot \rightarrow CH_3\cdot + CO_2\uparrow$

$2CH_3\cdot \rightarrow CH_3\text{-}CH_3\uparrow$

$CH_3\cdot \rightarrow CH_3^+ + e^-$

Since the decarboxylation of acetate anions required larger overpotentials (>1.23 V vs. SHE), electrolysis of water molecules ($2H_2O \rightarrow 4H^+ + 4e^- + O_2\uparrow$) will take place. Because the water concentration as a solvent [24] reached as high as 55.6 mol/L, the O_2 evolution from water seriously influenced the electro-oxidation efficiency of acetate anions at certain electrode potentials.

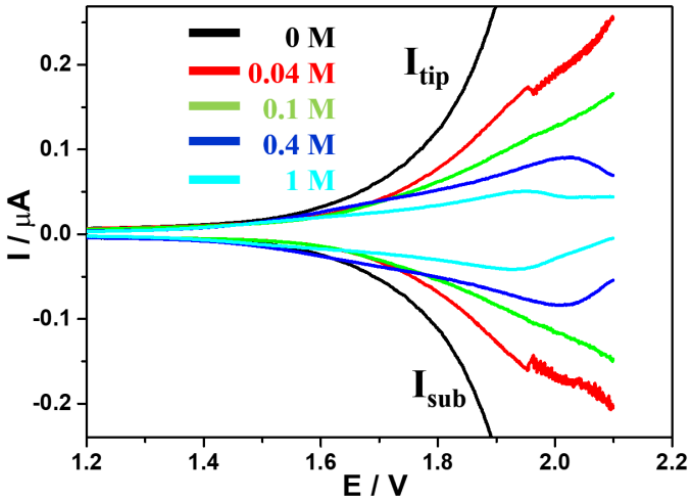

Figure 3. TG/SC LSV curves in 0.1 M $HClO_4$ electrolyte of acetate at different concentrations: 0 M (black), 0.04 M (red), 0.1 M (green), 0.4 M (blue), and 1 M (cyan). Conditions: E_{sub} of 0 V and scan rate of 50 mV/s.

In absence of acetate in 0.1 M $HClO_4$ electrolyte, the anodic scanning current at the tip was produced by OER of water. The current at the substrate was linked to the reduction of O_2 molecules. The high catalytic activity of Pt for both OER and ORR led to elevated efficiencies of generation and collection of O_2. As shown in the black trace of Figure 3, the ratio of I_{sub}/I_{tip} reached almost 100%. Meanwhile, the current reached greatest values in absence of acetates in the electrolyte when compared to other contrast curves obtained in the presence of acetate. In Figure 3, the current levels at the tip decreased as acetate concertation increased. The current disturbance in the red curve (0.04 M) was ascribed to the presence of large amounts of gas bubbles generated at more positive potentials. In other words, bubbles landed on the microelectrode surface and then left were the cause of current disturbances. At an acetate concentration of 0.4 M, a further decrease in I_{tip} was observed when compared to the value obtained at lower concentration of acetate. In particular, a transition in I_{tip} appeared at 2.04 V (blue curve in Figure 3), and I_{tip} kept decreasing at potentials above 2.04 V. Such a potential transition shifted negatively to 1.95 V when the acetate concentration was further raised to 1 M (cyan curve in Figure 3). In sum, TG/SC results showed a strong effect of acetate concentration on OER. In other words, higher concentrations of acetate led to lower currents of OER. The dynamic transition of OER was observed at high electrode potentials in $HClO_4$ electrolyte at elevated acetate concentrations.

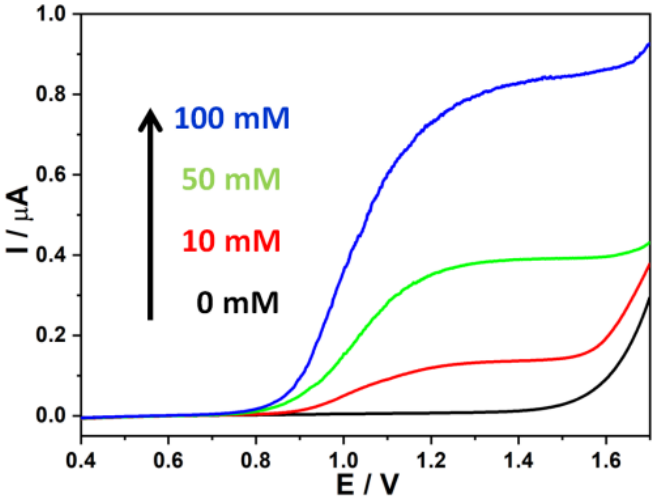

Figure 4. The effect of NaOH concentration on OER.

The changing trend of the anodic scanning current in Figure 3 was not only caused by the variation in acetate concentration but also pH since the acetate solution was alkaline. Therefore, further experiments using alkaline electrolytes were conducted. In 0.1 M $NaClO_4$ electrolyte, the onset potential of OER was around 1.4 V (black curve in Figure 4). Note that the presence of 10 mM NaOH in 0.1 M $NaClO_4$ electrolyte induced two transition potentials (red curve in Figure 4). The much smaller OER potential (0.91 V) corresponded to the oxidation of OH^- on Pt ($4OH^- \rightarrow O_2+2H_2O+4e^-$), and the greater potential (1.55 V) was linked to the oxidation of H_2O ($2H_2O \rightarrow O_2+4H^++4e^-$). The latter reaction was reasonable because higher electrode potentials could induce elevated reaction rates to produce local depletion regions without or trace OH^- near the Pt surface. Further increase in NaOH concentration to 50 mM (green curve) and 100 mM (blue curve) led to obvious enhancement in the oxidation current of OH^-, and the oxidation potential of H_2O slightly shifted to greater values.

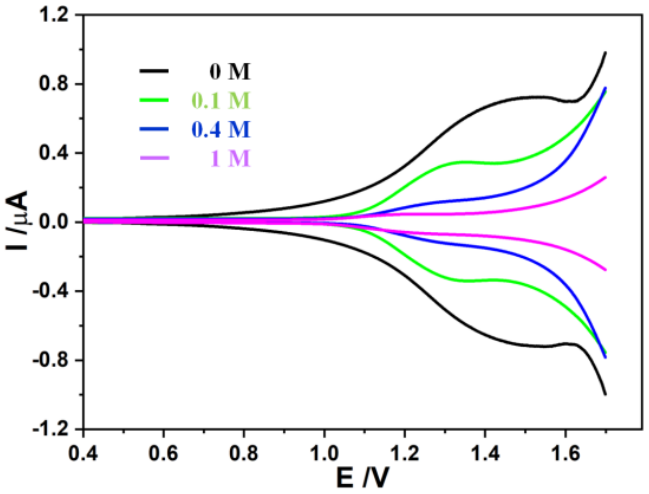

Figure 5. TG/SC LSV curves obtained at different acetate concentrations in 10 mM NaOH and 0.1 M $NaClO_4$ electrolyte. Black, green, blue and cyan curves correspond to 0, 0.1, 0.4 and 1 M acetate in the electrolyte, respectively. Conditions: E_{sub} of -0.6 V and scan rate of 50 mV/s.

Since acetate as a weak base did not significantly change the pH of the strong alkaline solution, 10 mM NaOH electrolyte was employed as a strong base to control the pH. Because Pt had different catalytic activities at different pH values, the collection potential value in the previous case was not applicable and a new value was required [25]. In LSV testing, -0.6 V was determined as the effective potential for ORR at the substrate but did not induce HER in the electrolyte containing 10 mM NaOH and 0.1 M $NaClO_4$. Hence, a potential value of -0.6 V was applied at the substrate to collect the O_2 generated from the tip. By adding different concentrations of acetate into the alkaline electrolyte, LSV curves were obtained during TG/SC scans (Figure 5). Clearly, the OER performance decreased as the concentration of acetate increased. These results were similar to those obtained in the acidic electrolyte.

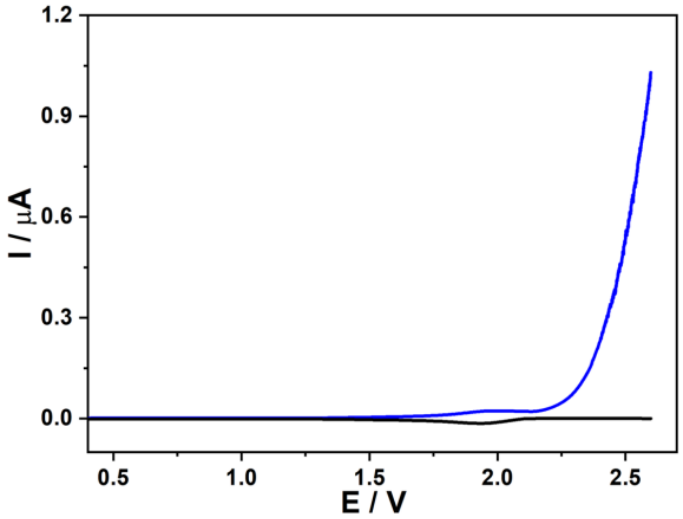

Figure 6. LSV TG/SC curves of 1 M acetate in 0.1 M $HClO_4$. Conditions: E_{sub} of -0.6 V and scan rate of 50 mV/s.

From TG/SC LSV results in acidic and alkaline electrolytes, high acetate concentrations and elevated electrode potentials jointly inhibited the OER. Thus, the electrode potential was further extended to 2.6 V using 1 M acetate in 0.1 M $HClO_4$. As shown in Figure 6, a bump was visible in LSV curves on both the tip and substrate. The upward bump obtained for the tip anodic scanning and downward bump observed for the substrate collection corresponded to the OER and ORR, respectively. Above 2.18 V, the OER was entirely inhibited because no ORR occurred at the substrate. Meanwhile, a dramatic current increase appeared for the tip above 2.18 V, which should be related to the oxidation of pure acetate without the occurrence of OER since no O_2 molecules were detected at the substrate. Therefore, OER occurred only at relatively low electrode potentials during acetate oxidation. At high electrode potentials, the OER reaction was inhibited, giving rise to only oxidation of acetate. The results associated with the inhibition of OER during acetate oxidation were consistent with previously reported literature and linked to the Kolbe reactants, oxygen-containing species, and adsorbed intermediates[20].

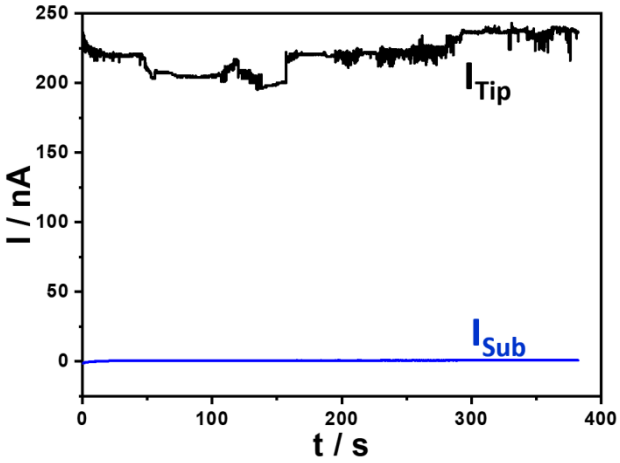

Figure 7. Chronoamperometry showing the inhibition effect at applied potentials of 2.4 V at the tip and -0.6 V at the substrate. Conditions: electrolyte containing 1 M acetate in 0.1 M $HClO_4$.

To further confirm the inhibition effect during TG/SC experiments, a high constant potential was held at 2.4 V for the tip and -0.6 V for the substrate (Figure 7). As evidenced by the ground level of I_{sub}, no O_2 was detected at the substrate. Thus, OER was completely inhibited at such high electrode potentials and elevated concentrations of acetate. The dramatic current fluctuation at the tip was caused by the large quantities of produced gas bubbles made of CO_2 and ethane, among others, consistent with data of Figure 6. All experimental results showed that OER can be effectively inhibited at joint conditions of elevated anodic potentials and high acetate concentrations. One reasonable explanation for such an inhibition phenomenon had to do with the decarboxylation, which predominated the reaction through intermediate adsorption [26]. More information about the origin of the inhibition cannot be provided since the present TG/SC technique cannot effectively detect other intermediates and products.

4. CONCLUSIONS

TG/SC mode in SECM was successfully employed for *in-situ* and real-time monitoring of oxygen evolution behavior during a typical Kolbe reaction. The OER dominated the oxidation current at lower oxidation potentials both in acidic and alkaline media. However, high electrode potentials and elevated acetate concentrations inhibited the OER, thereby improving the oxidation efficiency of acetate oxidation. Though TG/SC technique was found useful for *in-situ* and real-time detection of O_2 generated during the Kolbe reaction, other products (such as ethane and CO_2) cannot be detected like O_2. In sum, other reaction products, byproducts, or intermediates also played important roles in the reaction efficiency, which require future exploration using TG/SC technique.

ACKNOWLEDGEMENT
This work was financially supported by the Zhejiang Provincial Natural Science Foundation of China (Grant Nos. LQ20B010012 and LY20B030007).

References

1. J.-i. Yoshida, K. Kataoka, R. Horcajada, A. Nagaki, *Chem. Rev.*, 108 (2008) 2265.
2. F. Lebreux, F. Buzzo, I. Marko, *ECS Trans.*, 13 (2008) 1.
3. M. D. Karkas, *Chem. Soc. Rev.*, 47 (2018) 5786.
4. H. J. Schäfer, Kolbe Reactions, In *Comprehensive Organic Synthesis*, Trost, B. M.; Fleming, I., Eds. Pergamon: 1991.
5. T. Laue, A. Plagens, T. Laue, A. Plagens, *Kolbe Electrolytic Synthesis*. Blackwell Science: 2005.
6. J. Schwarz, B. König, *Green Chem.*, 20 (2018) 323.
7. R. Arrigo, M. Hävecker, M. E. Schuster, C. Ranjan, E. Stotz, A. Knop-Gericke, R. Schlögl, *Angew. Chem. Int. Ed.*, 52 (2013) 11660.
8. X. Peng, T. Omasta, X. Zhao, W. E. Mustain, *ECS Trans.*, 85 (2018) 29.
9. C. G. Zoski, *J. Electrochem. Soc.*, 163 (2016) H3088.
10. Allen J. Bard, M.V. Mirkin, *Scanning Electrochemical Microscopy*. CRC Press: 2012.
11. S. Amemiya, A. J. Bard, F.-R. F. Fan, M. V. Mirkin, P. R. Unwin, *Ann. Rev. Anal. Chem.*, 1 (2008) 95.
12. T. Kai, M. Zhou, Z. Duan, G. A. Henkelman, A. J. Bard, *J. Am. Chem. Soc.*, 139 (2017) 18552.
13. Q. Zhang, P. Liu, Z. Zhu, J. Zhang, F. Cao, *Corros. Sci.*, 164 (2020) 108312.
14. Q. Zhang, Z. Zhu, P. Liu, J. Zhang, F. Cao, *J. Electrochem. Soc.*, 166 (2019) C401.
15. Q. Zhang, Z. Ye, Z. Zhu, X. Liu, J. Zhang, F. Cao, *Corros. Sci.*, 139 (2018) 403.
16. X. Y. Wang, Y. Xia, Y. R. Zhou, L. L. Nie, F. H. Cao, J. Q. Zhang, C. N. Cao, *Acta Metall. Sin.*, 51 (2015) 631.
17. C. G. Zoski, *Electroanal.*, 14 (2002) 1041.
18. L. Johnson, D. A. Walsh, *J. Electroanal. Chem.*, 682 (2012) 45.
19. K. Eckhard, X. Chen, F. Turcu, W. Schuhmann, *Phys. Chem. Chem. Phys.*, 8 (2006) 5359.
20. A. K. Vijh, B. E. Conway, *Chem. Rev.*, 67 (1967) 623.
21. L. Eberson, *Electrochim. Acta*, 12 (1967) 1473.
22. V. A. Grinberg, Y. B. Vassiliev, *Russ. J. Electrochem.*, 32 (1996) 281.
23. D. F. A. Koch; R. Woods. *Electrochim. Acta*, 13 (1968) 2101.
24. L. Schulz, S. R. Waldvogel, *Synlett*, 30 (2019) 275.
25. X. Ge, A. Sumboja, D. Wuu, T. An, B. Li, F. W. T. Goh, T. S. A. Hor, Y. Zong, Z. Liu, *ACS Catal.*, 5 (2015) 4643.
26. B. E. Conway, B. V. Tilak, *Adv. Catal.*, 38 (1992) 1.